PHYSICAL REVIEW B

CONDENSED MATTER

THIRD SERIES, VOLUME 39, NUMBER 4 1 FEBRUARY 1989

Optical dephasing, hyperfine structure, and hyperfine relaxation associated with the 580.8-nm $^7F_0$-$^5D_0$ transition of europium in Eu^{3+}:Y_2O_3

W. R. Babbitt

High Technology Center, Boeing Electronics, P.O. Box 24969 MS:7J-27, Seattle, Washington 98124-6269

A. Lezama and T. W. Mossberg

Department of Physics and Chemical Physics Institute, University of Oregon, Eugene, Oregon 97403

(Received 25 May 1988)

We have employed spectral-hole-burning, coherent-transient, and optical-rf double-resonance techniques to measure various parameters associated with the 580.8-nm $^7F_0$-$^5D_0$ transition of Eu^{3+} doped into Y_2O_3. In particular, we have measured the hyperfine splittings of the terminal levels (for both ^{151}Eu and ^{153}Eu), an effective thermalization rate of the ground-state ($^7F_0$) hyperfine manifold over the temperature range of $\simeq$4–15 K, and the homogeneous linewidth of the optical transition over the range of $\simeq$14–35 K. Large ratios of inhomogeneous to homogeneous linewidth at elevated temperatures (10^3 at 25 K) and long ground-state hyperfine thermalization times (>30 h at 4 K) make this an interesting crystal in the context of spectrally addressable optical memories.

I. INTRODUCTION

Rare-earth atoms doped into various hosts are known to exhibit very sharp optical lines—especially at cryogenic temperatures.[1–3] In this context, the $^7F_0$-$^5D_0$ transition of the europium in Eu^{3+}:Y_2O_3 stands out because of its kilohertz-scale[4] homogeneous linewidth for temperatures in the range of 1 K. In the present paper, we present measurements of the homogeneous linewidth of this transition as a function of temperature. We also present measurements of effective population thermalization rates of the $^7F_0$ ground-state hyperfine sublevels as a function of temperature. Finally, we have measured the hyperfine splittings of both terminal levels of the transition. The narrowness of the optical transition and the stability of the hyperfine populations at relatively high temperatures make the $^7F_0$-$^5D_0$ transition of Eu^{3+}:Y_2O_3 interesting from the prospective of advanced frequency-selective optical memories.[5–8]

II. EXPERIMENTS

The $^7F_0$-$^5D_0$ 580.8-nm optical transition studied corresponds to Eu^{3+} ions located at C_2 symmetry sites.[9] The crystalline field at these sites is sufficiently nonsymmetric to relax the free-space selection rules forbidding the $J=0$ to $J=0$ transition under investigation. The crystal (2% Eu^{3+}:Y_2O_3) used is 5 mm in length. At liquid-helium temperatures the $^7F_0$-$^5D_0$ transition in this crystal displays roughly a 10-GHz inhomogeneous absorption width and a line-center weak signal absorption of 77%. Both of europium's almost equally abundant isotopes, ^{151}Eu and ^{153}Eu, have nuclear spin $I=\frac{5}{2}$. The nuclear quadrupole moment interacts with the electric field at the nucleus, splitting the electronic levels into triplets of doubly degenerate hyperfine levels. Measured[4] at the center of the inhomogeneous absorption profile, the 1.6 K homogeneous width of the $^7F_0$-$^5D_0$ transition is an extremely narrow 2.5 kHz.

A. Hyperfine structure

The hyperfine splittings of the ground ($^7F_0$) and excited ($^5D_0$) states of the two Eu isotopes were determined using a combination of optical-hole-burning[10] and optical-rf double-resonance techniques.[11] In the hole-burning experiments, a single-frequency standing-wave dye laser with $\simeq$2-MHz bandwidth, 15-μW power, and 80-μm spot size at the sample, was used to burn a hole near the center of the inhomogeneous absorption profile. A total exposure time of 10 sec was used to completely bleach the sample. The bleaching occurs because the population of a ground-state hyperfine level is depleted by the laser while the population of the two other hyperfine levels is enhanced. Following the burn cycle, the laser was attenuated in power by 1000 times and used to obtain an absorption spectrum in the spectral vicinity of the hole. Such a spectrum is shown in Fig. 1. The large transmis-

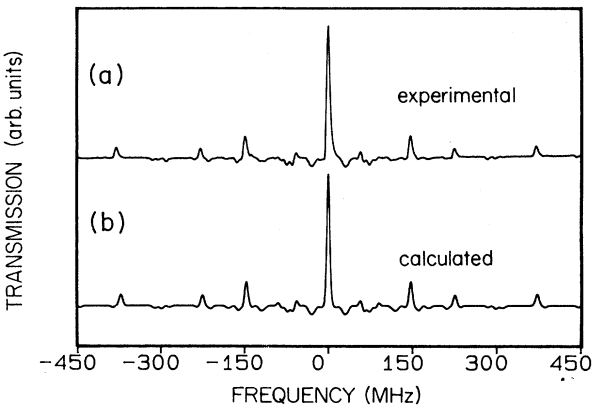

FIG. 1. Hole burning in a segment of the $^7F_0$-$^5D_0$ inhomogeneous absorption line of 2% Eu^{3+}:Y_2O_3 at 4.5 K. (a) Measured transmission spectrum. (b) Spectrum calculated using the hyperfine-level splittings given in Table I.

sion peak in the center of the trace corresponds to the frequency of the primary absorption hole. For each Eu isotope, three side holes and 21 antiholes corresponding, respectively, to decreased and enhanced absorption are expected on each side of the primary hole. The frequency separations between the primary hole and side holes yield the excited-state hyperfine splittings. Certain frequency intervals between the primary hole and the antiholes represent ground-state hyperfine level splittings, while others represent sum and difference frequencies of the excited-state and ground-state splittings. The relative depths of the holes and antiholes depend on the characteristics of the optical pumping cycle and the oscillator strengths of the transitions between upper- and ground-state hyperfine levels.

From the spectrum of Fig. 1(a) it is possible to deduce the frequencies of the excited-state hyperfine splittings. Observe that only four of the six expected side holes are clearly present in the spectrum. However, the almost doubled intensity of the second hole (from the central peak) indicates a peak overlap. It also turns out that another hole is not observed because of overlap with an antihole. Nevertheless, using the fact that for each isotope the sum of two of the splittings is equal to the third one, it is possible to deduce all six frequency splittings which are summarized in Table I.

The complexity of the antihole features makes it difficult to extract the ground-state hyperfine splittings. Instead, we have used an optical-rf double-resonance technique.[11] A narrow absorption hole was burned in the inhomogeneous profile. With the burning laser still on, fluorescence was measured as a function of the frequency of an applied rf field. When the rf was resonant with ground-state hyperfine transitions, increases in fluorescence intensity were produced. Six resonances were observed, and Fig. 2 shows the observed fluorescence signal corresponding to one of them. The noisy aspect of the spectrum is due to laser jitter producing occasional jumps of the laser frequency out of the burned hole and resulting in a large fluorescence increase. The observed resonances are listed in Table I, also listed are the observed linewidths which are probably due to inhomogeneous broadening of the hyperfine levels.

The consistency of the results of the hole-burning and optical-rf double-resonance measurements were checked by numerically simulating the hole-burning spectrum starting from the observed hyperfine splittings. We used a linear-absorption model, where the burned hole is supposed to be Gaussian in shape and to have a 8-MHz [full width at half maximum (FWHM)] linewidth. We also assumed that the population pumped out of one hyperfine sublevel was, after relaxing, equally distributed between the remaining two, and that the transition probabilities from the ground state to the excited state are the same for all possible pairs of hyperfine levels. The calculated spectrum is shown in Fig. 1(b). The differences in the peak intensities between this spectrum and the experimental one are due to the total neglect of the selection rules in our model. The overall agreement between the theoretical and observed spectrum confirms the hyperfine splitting assignment.

The knowledge of the hyperfine structures of the ground and excited states provides some information about the quadrupole electronic tensor for these states. From the observed splittings one can deduce the asymmetry parameter[12] η. Using the usual convention for which the quantization axis is chosen to correspond to the larger quadrupole moment, we obtain $\eta_g = 0.83$ and $\eta_e = 0.51$ for the ground and the excited states, respectively. The fact that both values are different from zero indicates a strong asymmetry of the electric field at the Eu nucleus. It should be pointed out that since the site symmetry is C_2, the ground and excited states need only to have one common quadrupole principal axis. Therefore, the above values of η refer, in principle, to different

TABLE I. Hyperfine level separation and linewidth for states $^7F_0$ and $^5D_0$ of $^{151}Eu^{3+}$ and $^{153}Eu^{3+}$ in 2% Eu^{3+}:Y_2O_3 at 4.5 K.

	^{151}Eu		^{153}Eu	
	ν (MHz)	$\Delta\nu_{FWHM}$ (MHz)	ν (MHz)	$\Delta\nu_{FWHM}$ (MHz)
$^7F_0$	29.35 (0.02)	0.17 (0.02)	73.3 (0.1)	0.4 (0.1)
	34.0 (0.05)	0.22 (0.02)	87.8 (0.2)	1.0 (0.2)
	63.3 (0.05)	0.14 (0.05)	161.1 (0.3)	1.2 (0.2)
$^5D_0$	58 (2)		147 (5)	
	89 (7)		225 (7)	
	147 (5)		372 (10)	

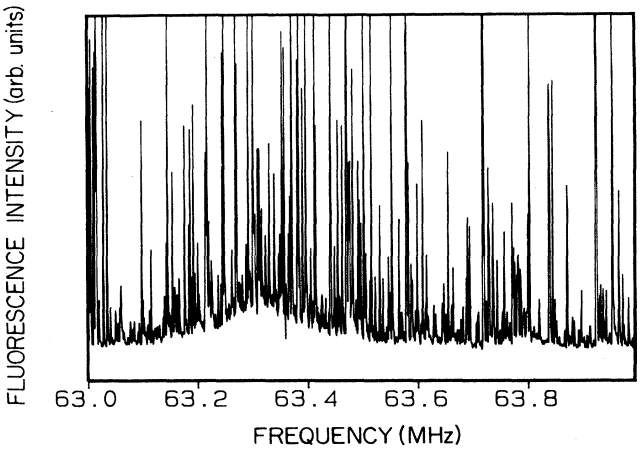

FIG. 2. Observed optical-fluorescence signal, as a function of the applied rf frequency. The resonance at 63.3 MHz corresponds to a ground-state–hyperfine transition of $^{151}Eu^{3+}$. The sharp features in this spectrum are due to laser jitter (see text).

choices of axes.[13] In fact, the observed hole-burning spectrum provides an indication that the axes are not the same. For a given choice of axes, it is possible to diagonalize the nuclear-quadrupole Hamiltonian[12] and then to calculate the overlap factors between excited- and ground-state nuclear eigenstates. If we assume that the axes are the same, this calculation results in strong approximate selection rules coupling a given hyperfine level of the ground (excited) state to one hyperfine level of the excited (ground) state. The observed spectrum showing antiholes at all possible frequency combinations is not consistent with such strong selection rules, indicating that the axes are not the same in the ground and excited states. Finally, we note that the ratio of the splittings of the two isotopes agrees well with the ratio of the nuclear-quadrupole moments [$Q(^{153}Eu)/Q(^{151}Eu)=2.54$] previously measured.[14]

B. Optical pumping and relaxation of ground-state sublevels

Illumination of the $^7F_0$-$^5D_0$ transition by two resonant laser-light pulses (referred to as pulses 1 and 2) optically delayed with respect to each other by time t_{21}, has the effect of creating a frequency-dependent population transfer between the ground- and excited-state hyperfine manifolds.[15] The magnitude of the population transfer oscillates in frequency space with period $1/t_{21}$. As the excited atoms relax via radiative decay (millisecond time scale), a frequency-dependent nonthermal population distribution (FDNTPD) among the ground-state hyperfine levels develops. In general, information can be encoded in the frequency dependence of the population modulation. The decay rate associated with the ground-state FDNTPD determines how long this information can be stored.

To measure an effective FDNTPD decay rate, the sample was illuminated by a series of laser-pulse pairs.[16] The pulses within each pair were temporally separated by t_{21}, and pulse pairs were repeated at 5–10 Hz. Successive pulse pairs had the effect of increasing the amplitude of the ground-state FDNTPD. After terminating the train of excitation pulse pairs, the amplitude of the ground-state FDNTPD was measured using stimulated echo techniques.[15,16] In particular, after various delays, attenuated readout pulses were employed to generate stimulated echo signals. The intensity of each echo signal is proportional to the squared amplitude of the ground-state FDNTPD then present in the sample.

An excimer-pumped, pulsed dye laser (up to 10-Hz repetition rate) was used to produce the light pulses described above. The dye-laser pulses had a temporal FWHM of 4 nsec, a spectral width of $\simeq 5$ GHz, and frequency jitter of ± 3 GHz. The dye-laser output was optically divided and delayed to achieve pulse-pair separations, t_{21}'s, of up to 425 nsec. Mechanical shutters in each path were used to determine whether one or two pulses from each pair would illuminate the crystal. The two light beams were recombined and focussed to a 100-μm spot at the crystal. Pulses employed to generate a ground-state FDNTPD had peak powers of $\simeq 1$ kW at the crystal. At this power level, it was observed that single pulses did not saturate the transition. Pulses used to generate stimulated echoes and thereby measure the ground-state FDNTPD were attenuated to have peak powers of $\simeq 10$ W. After the crystal, the light beams were collimated and sent through a dual Pockels-cell-type optical shutter. This shutter, which extinguished the input pulses, was gated open to transmit the echo signals. The integrated intensity of each detected echo signal was recorded and stored. Decay rates measured were found to be independent of pulse intensities and laser repetition rates.

For temperatures above 12.5 K, the ground-state FDNTPD was found to decay on time scales of less than a minute, and the following experimental procedure was employed. A FDNTPD was achieved by illuminating the sample with a series of pulse pairs ($t_{21}=22$ nsec). Thereafter, a train of single pulses was employed to generate stimulated echoes, and the decay of individual echoes versus time was recorded. Data obtained from numerous repetitions of the same procedure were averaged and fit to an exponential decay function. Results are shown in Fig. 3. It should be noted that the FDNTPD decays at half the rate of the stimulated echo intensity.

For lower temperatures, the FDNTPD decay rate decreases dramatically and a different measurement procedure was employed. Following the build up of a ground-state FDNTPD as described above, a train of up to 400 stimulated echoes (which required up to 40 sec) was produced at various delay intervals. Exponential decay rates were determined by fitting to the measured decay of the train-averaged echo intensity versus time. In all cases, the echo-train durations were set much smaller than the relaxation time under study. The above procedure was repeated for temperatures ranging from 4.5 to 12.3 K and for $t_{21}=22$ and 400 nsec. The results are shown in Fig. 3. No difference was detected between the decay rates measured with $t_{21}=22$ nsec and $t_{21}=400$ nsec, suggesting that there is no significant spectral

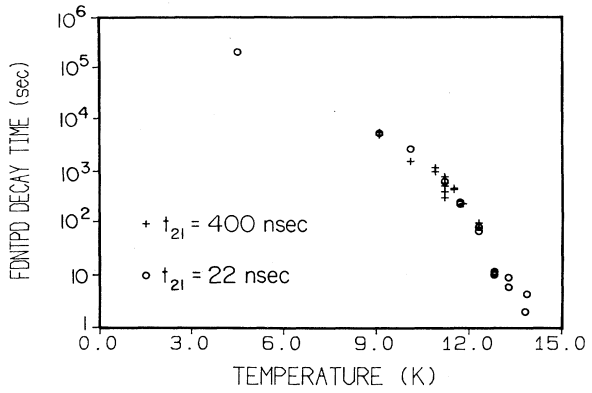

FIG. 3. Ground-state ($^7F_0$) frequency-dependent nonthermal population distribution decay rate of 2% Eu^{3+}:Y_2O_3 as a function of temperature. The results obtained for two different values of t_{21} are reported.

diffusion of the ground-state FDNTPD over frequency intervals larger than (400 nsec)$^{-1}$.

The two measurements of the long FDNTPD relaxation time at 4.5 K were made by comparing the intensity of the stimulated echoes generated shortly after a FDNTPD was built with the intensity of echoes generated after a $\simeq$13 h delay. The stimulated echo intensity decreased to 60±20 % of its original value over this period, corresponding to a $1/e$ FDNTPD amplitude relaxation time of 80±50 h. The actual relaxation time at 4.5 K may be considerably longer since there are other factors (such as beam misalignment) which might contribute to decreases in echo intensities on the time scale of 13 h.

It should be noted that the relaxation times for the populations of the different hyperfine levels may not be identical. If this were the case, one would expect to see a complicated multiexponential decay of the stimulated echo intensity as a function of time. In most cases, single-exponential decay provided a good description of our measured echo-decay curves; nevertheless, the adequacy of a single decay rate in describing the FDNTPD decay in this system needs further investigation. Pending the outcome of such an investigation, our measured decay rates should best be thought of as *effective* decay rates.

C. Homogeneous linewidth measurements

The homogeneous decay time of the $^7F_0$-$^5D_0$ transition as a function of temperature was determined by measuring[17] the temperature dependence of the intensity of the two-pulse photon echo, I_{PE}, for fixed excitation pulse temporal separation, t_{21}. This measurement is complicated at low tempertures (below 14 K) because of the long ground-state FDNTPD relaxation times. At these temperatures, any attempt to repeat a two-pulse echo measurement produces at a time t_{21} after the second pulse, in addition to the echo of the first pulse, a stimulated echo from all previous pulse pairs present in the sample within the ground-state FDNTPD relaxation time (a few days at the lowest temperatures). However, at temperatures greater than 14 K, the echoes stimulated from the ground-state FDNTPD decay rapidly and do not lead to appreciable stimulated echo intensities at the 10-Hz repetition rate employed. Fortunately, for the t_{21} values studied, the decay of the photon-echo intensity versus temperature above 14 K provides the most useful information.

In measuring the decay of echo intensity with temperature, the temperature was raised in steps from $\simeq$4 K up to a value at which the two-pulse photon echo signal became comparable to the background, and was then lowered stepwise to its original value. After each temperature step, the echo intensity $I_{PE}(T)$ was averaged over 400 echoes and recorded. In Figs. 4 and 5, a set of data obtained with $t_{21}=22$ nsec (400 nsec) is displayed. Two additional sets of data with $t_{21}=22$ nsec were obtained which produced results similar to the data displayed in Fig. 4.

The intensity of the photon echo as a function of temperature can be written in the form

$$I_{PE}(T)=I_0(t_{21})\exp\left[-4t_{21}/T_2(T)\right], \quad (1)$$

where $T_2(T)$ is the homogeneous decay time ($\Delta\nu_h=1/\pi T_2$) at temperature T. The proportionality constant $I_0(t_{21})$ depends on the experimental conditions and can have a nonexponential dependence on t_{21} (i.e., quantum beats).[13] However, with the experimental conditions and t_{21} fixed, $I_0(t_{21})$ can be considered constant and independent of temperature. This assumes that the homogeneous decay time is the only temperature-dependent parameter which affects the intensity of the photon echo.

As was measured by Macfarlane and Shelby (Ref. 4), the nonphonon contribution to the homogeneous width at absorption line center is only 2.5 kHz. Phonon-induced broadening can occur via several processes,[18] but because the terminal levels of the $^7F_0$-$^5D_0$ transition are energetically isolated, the dominant process mechanism

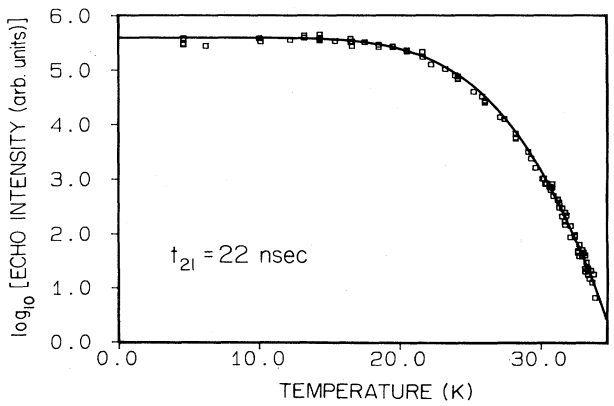

FIG. 4. Two-pulse photon-echo intensity as a function of temperature with $t_{21}=22$ nsec. The solid line represents a fit of the data to Eqs. (1) and (2) for $\Theta_D=230$ K and $H=210\times10^9$ sec^{-1}.

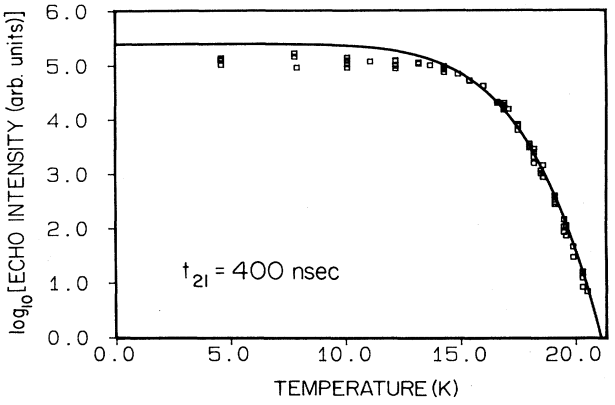

FIG. 5. Two-pulse photon-echo intensity as a function of temperature with $t_{21}=400$ nsec. The solid line represents a fit of the data to Eqs. (1) and (2) for $\Theta_D=230$ K and $H=210\times10^9$ sec^{-1}.

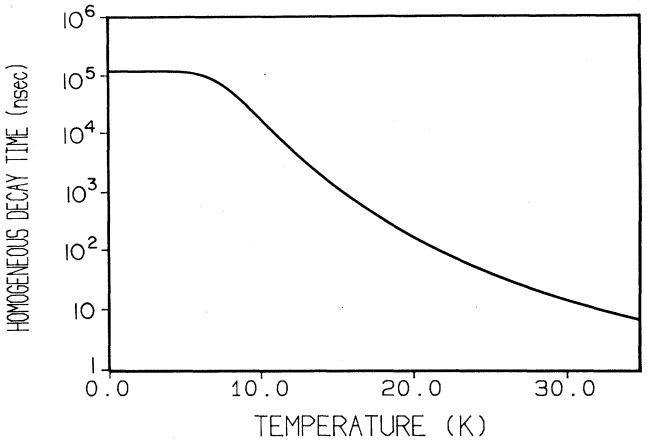

FIG. 7. Homogeneous decay time of the $^7F_0$-$^5D_0$ transition of Eu^{3+}:Y_2O_3 vs temperature, calculated from Eq. (2) for $\Theta_D=230$ K and $H=210\times10^9$ sec^{-1}. The low-temperature value was set according to the measurements of Ref. 4.

in the present case is expected to be the two-phonon Raman process.[18–21] Provided the electron-phonon coupling is sufficiently weak,[21] we should be able to write

$$\frac{1}{T_2(T)}=\frac{1}{T_2(T=0)}+H(T/\Theta_D)^7\int_0^{\Theta_D/T}dx\frac{x^6e^x}{(e^x-1)^2}\ , \tag{2}$$

where $T_2(T=0)$ is the low temperature, nonphonon contribution to the homogeneous decay time (130 μsec), Θ_D is the Debye temperature of the crystal, and H is the phonon-electron coupling parameter. The dominant dependence of T_2 on T is given by the $(T/\Theta_D)^7$ factor. However, as seen in Fig. 6, there is a significant departure from a T^7 law of the logarithm of the observed echo intensity with $t_{21}=22$ nsec. This indicates that, in the present case, the Debye temperature is low enough to allow the integral in expression (2) to vary appreciably over the considered temperature range. Consequently, both H and Θ_D can be deduced from our data with $t_{21}=22$ nsec. From a least-squares fit of our data to Eqs. (1) and (2), we obtain $\Theta_D=230\pm30$ K and values of H on the order of 2×10^{11} sec.$^{-1}$.[22] A fit of our data with $t_{21}=400$ nsec is consistent with these values. The Debye temperature measured here is comparable to values deduced by other means.[23] Because of the problems mentioned above, only the data for $T>14$ K was used in the fitting procedures. Using the values of Θ_D and H given above, we have calculated the solid lines plotted in Figs. 4–6 and the variation of the homogeneous decay time T_2 with temperature shown in Fig. 7. The $T=0$ intercept of the plot in Fig. 7 was set using the measurement of Ref. 4.

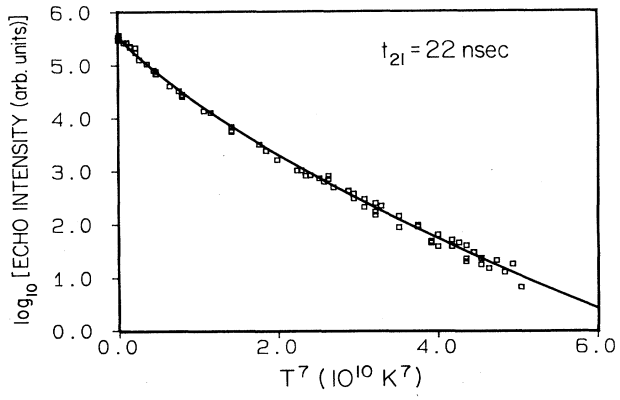

FIG. 6. Two-pulse photon-echo intensity plotted as a function of the seventh power of the temperature. The solid line represents a fit of the data to Eqs. (1) and (2) for $\Theta_D=230$ K and $H=210\times10^9$ sec^{-1}. The data sets shown here and in Fig. 4 are the same.

III. CONCLUSION

In summary, the hyperfine splittings of the $^{151}Eu^{3+}$ and $^{153}Eu^{3+}$ isotopes doped into Y_2O_3 have been determined for the $^5D_0$ and $^7F_0$ energy levels. An effective relaxation time of the FDNTPD produced in the $^7F_0$ ground-state hyperfine levels was measured over the temperature range of 4.5 to 14 K and was found to vary from a few seconds to a few days, suggesting that long term storage of information in ground-state FDNTPD is possible. The optical homogeneous decay rates were measured up to 35 K and the phonon-electron coupling parameter and the Debye temperature were deduced.

ACKNOWLEDGMENTS

We gratefully acknowledge financial support from the U.S. Army Research Office under Contract No. DAAL-03-89-K-0004 and from Conselho Nacional de Desenvolvimento Científico e Tecnológico (Brazil). We thank R. M. Macfarlane for the loan of the Eu:Y_2O_3 crystal.

[1]P. Hill and S. Hufner, Z. Phys. **240**, 168 (1970).
[2]*Laser Spectroscopy of Solids,* edited by W. M. Yen and P. M. Selzer (Springer-Verlag, Berlin, 1981).
[3]S. Hufner, *Optical Spectra of Transparent Rare Earth Compounds* (Academic, New York, 1978).
[4]R. M. Macfarlane and R. M. Shelby, Opt. Commun. **39**, 169 (1981).
[5]W. E. Moerner, J. Mol. Electron. **1**, 55 (1985).
[6]T. W. Mossberg, Opt. Lett. **7**, 77 (1982).
[7]W. R. Babbitt, Y. S. Bai, and T. W. Mossberg, in *Proceedings of the SPIE—The International Society for Optical Engineering,* edited by D. R. Pape (SPIE, Bellingham, 1986), Vol. 639, p. 240.
[8]G. Castro, D. Haarer, R. M. Macfarlane, and H. P. Trommsdorff, U.S. Patent No. 4 101 976 (July 18, 1978).
[9]J. Heber, K. H. Hellwege, U. Kobler, and H. Murmann, Z. Phys. **237**, 189 (1970).
[10]L. E. Erickson, Phys. Rev. B **16**, 4731 (1977).
[11]L. E. Erickson, Opt. Commun. **21**, 147 (1977).
[12]A. Abragam, *The Principles of Nuclear Magnetism* (Oxford University Press, London, 1961).
[13]Y. C. Chen, K. Chiang, and S. R. Hartmann, Phys. Rev. B **21**, 40 (1980).
[14]K. Krebs and R. Winkler, Naturwissenschaften **21**, 490 (1960).
[15]T. W. Mossberg, R. Kachru, S. R. Hartmann, and A. M. Flusberg, Phys. Rev. A **20**, 1976 (1979).
[16]W. H. Hesselink and D. A. Wiersma, Phys. Rev. Lett. **43**, 1991 (1979).
[17]T. Kohmoto, H. Nakatsuka, and M. Matsuoka, Jpn. J. Appl. Phys. **22**, 6571 (1983).
[18]R. Orbach, Proc. R. Soc. London, Ser. A **264**, 458 (1961).
[19]D. E. McCumber and M. D. Sturge, J. Appl. Phys. **34**, 1682 (1963).
[20]W. M. Yen, W. C. Scott, and A. L. Schawlow, Phys. Rev. **136**, A271 (1964).
[21]D. Hsu and J. L. Skinner, J. Chem. Phys. **83**, 2097 (1985); **83**, 2107 (1985); **81**, 1604 (1984).
[22]The electron-phonon coupling parameter W of Ref. 21 can be calculated from these values. We obtain $W \simeq 0.06$, therefore justifying the use of Eq. (2).
[23]H. W. Goldstein, E. F. Neilson, P. N. Walsh, and D. White, J. Phys. Chem. **63**, 1445 (1959).